Chinese Journal of Natural Medicines

Discovery and characterization of naturally occurring covalent inhibitors of SARS-CoV-2 M^{pro} from the antiviral herb Ephedra

Qing HU, Yiwen ZHANG, Pengcheng CHEN, Yani ZHANG, Guanghao ZHU, Wei LIU, Chaoran WANG, Shuilian ZHENG, Nonger SHEN, Haonan WANG, Ping HUANG, Guangbo GE

Citation: Qing HU, Yiwen ZHANG, Pengcheng CHEN, Yani ZHANG, Guanghao ZHU, Wei LIU, Chaoran WANG, Shuilian ZHENG, Nonger SHEN, Haonan WANG, Ping HUANG, Guangbo GE, Discovery and characterization of naturally occurring covalent inhibitors of SARS-CoV-2 M^{pro} from the antiviral herb Ephedra, Chinese Journal of Natural Medicines, 2024, 22(9), 797-807. doi: 10.1016/S1875-5364(24)60577-7.

View online: https://doi.org/10.1016/S1875-5364(24)60577-7

Available online at www.sciencedirect.com
ScienceDirect
Chinese Journal of Natural Medicines 2024, **22**(9): 797-807
doi: 10.1016/S1875-5364(24)60577-7
Chinese Journal of Natural Medicines

•Original article•

Discovery and characterization of naturally occurring covalent inhibitors of SARS-CoV-2 M^{pro} from the antiviral herb Ephedra

HU Qing[1Δ], ZHANG Yiwen[1Δ], CHEN Pengcheng[1], ZHANG Yani[2], ZHU Guanghao[2], LIU Wei[3], WANG Chaoran[4], ZHENG Shuilian[1], SHEN Nonger[1], WANG Haonan[2], HUANG Ping[1*], GE Guangbo[2*]

[1] *Center for Clinical Pharmacy, Cancer Center, Department of Pharmacy, Zhejiang Provincial People's Hospital (Affiliated People's Hospital), Hangzhou Medical College, Hangzhou 310014, China;*
[2] *Shanghai Frontiers Science Center of TCM Chemical Biology, Institute of Interdisciplinary Integrative Medicine Research, Shanghai University of Traditional Chinese Medicine, Shanghai 201203, China;*
[3] *Shuguang Hospital Affiliated to Shanghai University of Traditional Chinese Medicine, Shanghai 200021, China;*
[4] *Dalian Institute of Chemical Physics, Chinese Academy of Sciences, Dalian 116023, China*

Available online 20 Sep., 2024

[ABSTRACT] The Chinese herb Ephedra (also known as Mahuang) has been extensively utilized for the prevention and treatment of coronavirus-induced diseases, including coronavirus disease 2019 (COVID-19). However, the specific anti-SARS-CoV-2 compounds and mechanisms have not been fully elucidated. The main protease (M^{pro}) of SARS-CoV-2 is a highly conserved enzyme responsible for proteolytic processing during the viral life cycle, making it a critical target for the development of antiviral therapies. This study aimed to identify naturally occurring covalent inhibitors of SARS-CoV-2 M^{pro} from Ephedra and to investigate their covalent binding sites. The results demonstrated that the non-alkaloid fraction of Ephedra (ENA) exhibited a potent inhibitory effect against the SARS-CoV-2 M^{pro} effect, whereas the alkaloid fraction did not. Subsequently, the chemical constituents in ENA were identified, and the major constituents' anti-SARS-CoV-2 M^{pro} effects were evaluated. Among the tested constituents, herbacetin (HE) and gallic acid (GA) were found to inhibit SARS-CoV-2 M^{pro} in a time- and dose-dependent manner. Their combination displayed a significant synergistic effect on this key enzyme. Additionally, various techniques, including inhibition kinetic assays, chemoproteomic methods, and molecular dynamics simulations, were employed to further elucidate the synergistic anti-M^{pro} mechanisms of the combination of HE and GA. Overall, this study deciphers the naturally occurring covalent inhibitors of SARS-CoV-2 M^{pro} from Ephedra and characterizes their synergistic anti-M^{pro} synergistic effect, providing robust evidence to support the anti-coronavirus efficacy of Ephedra.

[KEY WORDS] Main protease; Ephedra; Ephedra non-alkaloid fraction; Covalent inhibitors; Synergistic effect
[CLC Number] R965 **[Document code]** A **[Article ID]** 2095-6975(2024)09-0797-11

Introduction

The emergence of Severe Acute Respiratory Syndrome Coronavirus 2 (SARS-CoV-2) has transformed coronavirus disease 2019 (COVID-19) into a global health crisis [1]. Common symptoms of COVID-19, such as fever, cough, and fatigue, significantly impair patients' quality of life, particularly among the elderly and those with chronic conditions [2-4]. Consequently, it is crucial to identify effective and safe therapies to alleviate these symptoms and prevent further deterioration in patients' quality of life. In response to this challenge, a suite of proprietary Chinese medicines (CMs), including Maxing Shigan decoction, Qingfei Paidu decoction, and Lianhua Qingwen capsule, have been widely used to ameliorate the main symptoms of COVID-19. Increasing evidence has shown that these anti-COVID-19 CMs demon-

[Received on] 23-Oct.-2023
[Research funding] This work was supported by the National Key Research and Development Program of China (No. 2022YFC3502000), the Basic Public Welfare Research Program of Zhejiang Province (No. LGF22H280012), Zhejiang Provincial TCM Science and Technology Plan Project (Nos. 2023ZR064, GZY-ZJ-KJ-24004, 2024ZL007 and 2022ZB017), the Medical Science and Technology Project of Zhejiang Province (Nos. 2022495401, 2021KY040 and 2022KY069), Zhejiang Provincial Key Projects in Chinese Medicine (Nos. 2020ZZ003 and 2021ZZ001). Shanghai Science and Technology Innovation Action Plans (Nos. 21S21900600). Zhejiang Province "Ten Thousand People Plan" Science and Technology Innovation Leading Talents Project (No. 2020R52029).
[*Corresponding author] E-mails: huangping@hmc.edu.cn (HUANG Ping); geguangbo@shutcm.edu.cn (GE Guangbo)
[Δ]These authors contributed equally to this work.
These authors have no conflict of interest to declare.

strate promising health-promoting effects and high safety profiles [5, 6], encouraging further investigation into their active substances and mechanisms of action.

Notably, the most frequently used anti-COVID-19 CMs in China are derived from the famous herbal formula "Maxing Shigan decoction", in which Ephedra is recognized as a key antiviral herb [7-9]. Ephedra (stem of *Ephedra sinica*), also known as Mahuang in Chinese, is a preferred ingredient for preparing renowned anti-COVID-19 herbal medicines due to its antipyretic and analgesic properties, as well as its potential to improve lung function and alleviate asthma symptoms (Table S1) [10, 11]. However, the anti-SARS-CoV-2 compounds within Ephedra and their mechanisms of action have not been fully characterized, prompting further investigation into the antiviral substances of this herb.

The ongoing mutation of new coronaviruses (CoVs) poses a significant threat to vaccine efficacy and leads to variant-mediated resistance [12]. This underscores the urgent need to develop safer and more efficient therapeutics to combat COVID-19 [13, 14]. Among the various therapeutic targets for COVID-19, the highly conserved SARS-CoV-2 main protease (M^{pro}), also known as 3-chymotrypsin-like cysteine protease ($3CL^{pro}$), plays a pivotal role in proteolytic processing during the viral life cycle. Consequently, M^{pro} is a key target for the development of anti-CoV therapies [15, 16]. Phytochemicals found in CMs are a primary strategy for developing drug candidates [16]. Numerous natural compounds, particularly those bearing electrophilic moieties (e.g., *o*-quinone or Michael receptor), have the potential to covalently bind to SARS-CoV-2 M^{pro} [17]. For instance, Zhang *et al.* reported a comprehensive method for efficiently discovering and characterizing covalent SARS-CoV-2 M^{pro} inhibitors from CMs using chemoproteomic profiling of cysteine-modified peptides [18]. Additionally, certain flavonoids with catechol groups, such as myricetin and its analogs, have been found to covalently bind to key cysteines of SARS-CoV-2 M^{pro} [16]. Compared to classical reversible inhibitors, irreversible covalent inhibitors offer inherent advantages, including longer duration of action, more potent therapeutic efficacy *in vivo*, and reduced likelihood of drug resistance emergence [19].

This study aimed to uncover the naturally occurring covalent inhibitors of SARS-CoV-2 M^{pro} from Qingfei Paidu decoction, a newly approved CM for treating COVID-19. The objectives included identifying the covalently modified sites and revealing the underlying anti-SARS-CoV-2 M^{pro} mechanisms. To achieve these goals, the anti-SARS-CoV-2 M^{pro} effects of twenty-one herbs used in the preparation of Qingfei Paidu decoction were individually tested. The results demonstrated that *Ephedra sinica* extract (ESE) exhibited a significant inhibitory effect against SARS-CoV-2 M^{pro}. Furthermore, the non-alkaloid fraction isolated from Ephedra showed potent anti-SARS-CoV-2 M^{pro} effects in a time- and dose-dependent manner, while the alkaloid fraction did not inhibit SARS-CoV-2 M^{pro}. A comprehensive chemical analysis was conducted to identify the chemical constituents in the Ephedra non-alkaloid fraction (ENA), followed by testing the anti-SARS-CoV-2 M^{pro} effects of the major phytochemicals in ENA individually. Among all tested constituents, herbacetin (HE) and gallic acid (GA) displayed the most potent anti-SARS-CoV-2 M^{pro} effects. Notably, their combined use exhibited a significant synergistic effect against SARS-CoV-2 M^{pro}. These findings prompted further investigation into the anti-M^{pro} mechanisms of these two natural compounds using a range of techniques, including inhibition kinetic assays, mass spectrometry-based chemoproteomic profiling of cysteine-modified peptides, covalent docking, and molecular dynamics simulations.

Materials and Methods

Materials and reagents

ESE was provided by Jointown (Wuhan, China). Ephedra alkaloid and Ephedra non-alkaloid fraction (ENA) were isolated and prepared from Ephedra. The methods for expressing and purifying SARS-CoV-2 M^{pro} were followed as previously described (Fig. S1) [16]. Tryptone (LP0042) and yeast extract (LP0021) were supplied by Oxoid (England). Phenylmethylsulfonyl fluoride (PMSF) and Ni-NTA agarose were obtained from Qiagen (Germany). Lysozyme (64006060), imidazole (30104916), and dithiothreitol (DTT, 63002632) were obtained from Sinopharm (Shanghai, China). SuperNuclease (SSNP01) was ordered from Yiqiao Shenzhou (Beijing, China). EDTA disodium salt dihydrate was acquired from Amresco (USA). Trypsin, chymotrypsin, iodoacetamide (IAA), urea, HEPES, and NH_4HCO_3 were purchased from Sigma-Aldrich. Ferulic acid was ordered from TITAN (Shanghai, China). HE, catechin, myricetin, and epicatechin were procured from Shanghai Standard Technology Co., Ltd. Additionally, vitexin, isovitexin, tricin, rutin, quercitrin, isoquercitrin, naringenin, taxifolin, kaempferol, apigenin, quercetin, and GA were purchased from Chengdu Pufei De (Chengdu, China). Ebselen and dihydromyricetin were provided by TCI (Shanghai, China). Dabcyl-KNSTLQSG-LRKE-Edans (DKE), used as a fluorescence substrate, was synthesized by Genscript (Nanjing, China) and dispensed with ultrapure water. The purity of these standard compounds was greater than 98%. Formic acid, acetonitrile, dimethyl sulfoxide (DMSO), and methanol were provided by Fisher Scientific (Fairfield, USA). The reaction buffer, composed of 25 $mmol \cdot L^{-1}$ Tris-HCl (pH 7.4) and 1 $mmol \cdot L^{-1}$ EDTA, was prepared using Milli-Q water (Millipore, Bedford, USA). Each inhibitor was diluted in DMSO, and the solution was stored at −30 °C until needed for use.

SARS-CoV-2 M^{pro} inhibition assay

For the inhibitory activity assays of SARS-CoV-2 M^{pro} in a 96-well plate, a fluorogenic peptide DKE was used as the substrate. Dihydromyricetin, a known naturally occurring M^{pro} inhibitor, and ebselen, a synthetic M^{pro} inhibitor, were used as positive controls [17, 20]. Briefly, the reaction mixture (90 μL) contained SARS-CoV-2 M^{pro} (4 $\mu g \cdot mL^{-1}$ final concentration), reaction buffer, and each of the tested inhibitors

or DMSO. After preincubating the reaction mixtures for various periods (3 or 60 min) at 37 °C, 10 μL of the fluorescent substrate (20 μmol·L^{-1} final concentration) was added to initiate the enzymatic reaction. Fluorescence signals were continuously monitored using a multi-mode microplate reader (SpectraMax® iD3, Molecular Devices, Austria) with excitation/emission wavelengths of 340 nm/490 nm.

Identification of the major bioactive constituents in ENA

The constituents in the ENA were identified using a UHPLC-Q-Exactive Orbitrap system (Thermo Fisher Scientific, Grand Island, NY, USA) equipped with a Thermo Scientific Dionex Ultimate 3000 Series RS pump, a Dionex Ultimate 3000 Series TCC-3000RS column compartment, and a WPS-3000 autosampler. Chromatographic analysis was performed at 40 °C on an Acquity UPLC® BEH C18 column (2.1 mm × 100 mm, 1.7 μm) at a flow rate of 0.3 mL·min^{-1}. The mobile phases consisted of methanol (mobile phase A) and 0.1% formic acid (mobile phase B), with the following gradient elution: 0–2 min, 4% A; 2–6 min, 4%–12% A; 6–38 min, 12%–70% A; 38–38.5 min, 70% A; 38.5–39 min, 70%–95% A; 39–43 min, 95% A; 43–45 min, 4% A. The mass spectrometer Q-Exactive Orbitrap system was connected to the UHPLC system *via* heated electrospray ionization (H-ESI). The electrospray ionization source was optimized in both negative and positive ionization modes with the following parameters: auxiliary gas flow rate of 13 arbitrary units, capillary temperature of 300 °C, sheath gas (N2) flow rate of 35 arbitrary units, and spray voltage of 2.5 kV (negative mode) or 3.5 kV (positive mode). The scan mode utilized was Full MS/dd-MS^2, which includes one first-level full scan (resolution 70,000 FWHM) and one data-dependent secondary scan (resolution 17 500 FWHM) with a scanning range of *m/z* 80–1200. The collision energy gradient was set at 20, 50, and 100 V.

Identification of the covalent binding sites by biomass spectrometry

To elucidate the inactivation mechanisms of HE and GA against SARS-CoV-2 M^{pro}, the covalently modified sites on SARS-CoV-2 M^{pro} by these inhibitors were identified by analyzing the peptides of the target enzyme with and without inhibitor co-incubation. This identification process was conducted using the nanoLC-MS/MS system (EASY-nLC 1200, Thermo Fisher Scientific, USA), which records peptide signals in intact (MS^1) and fragmented (MS^2) forms, enabling comprehensive analysis of the modified peptides and modification sites [15, 16]. In brief, SARS-CoV-2 M^{pro} (100 μg) was co-incubated with HE or GA overnight at 37 °C. The mixtures were then denatured using 6 mol·L^{-1} urea for 10 min at 75 °C, reduced with 1 mmol·L^{-1} dithiothreitol at 95 °C for 10 min, and alkylated in the dark with 3 mmol·L^{-1} iodoacetamide for 30 min. Following this, ice-cold acetonitrile was added, and the samples were centrifuged at 16 000 *g* for 15 min. The proteins were then redissolved in an ammonium bicarbonate solution and digested with a mixture of chymotrypsin and trypsin at an enzyme-to-substrate ratio of 1 ∶ 40 (*W/W*) overnight at 37 °C. The digestion was terminated with formic acid at a final concentration of 1%. The samples were desalted using a Solid Phase Extraction Cartridge (MonoSpin C_{18}, GL Sciences), dried with a vacuum pump, and reconstituted for nanoLC-MS analyses.

A Hybrid Quadrupole-Orbitrap mass spectrometer (Q Exactive^{TM} HF-X, ThermoFisher Scientific, USA) was used to analyze the samples. Tryptic peptides (0.5–1 μg) were injected into the nanoLC-MS/MS system and separated on a self-packed analytical C_{18} column (20 μm × 360 μm × 200 mm, 3 μm) at a flow rate of 300 nL·min^{-1}. The mobile phases were water with 0.1% formic acid (solvent A) and 80% acetonitrile with 0.1% formic acid (solvent B), with the following elution gradient: 0–1 min, 1%–6% B; 1–47 min, 6%–35% B; 47–54 min, 35%–37% B; 54–56 min, 37%–95% B; 56–65 min, 95% B. The mass spectrometry data were acquired in data-dependent mode on the Q Exactive^{TM} HF-X, scanning from *m/z* 375 to 1800 with a resolution of 60 000, an automatic gain control (AGC) target of 3 × 10^6, and a maximum injection time (IT) of 50 ms. Fragmentation was performed in Higher Energy Collision Dissociation (HCD) mode with a resolution of 15 000 at 28% normalized collision energy (AGC target of 1× 10^5, maximum IT of 30 ms). The protein database of SARS-CoV-2 M^{pro} was used for analysis, defining trypsin and chymotrypsin as cleavage enzymes. Carbamidomethylation of cysteine, $C_{15}H_{10}O_7$ or $C_7H_6O_5$ adducts on cysteine, and oxidation of methionine were considered as dynamic modifications. Accurate mass measurements were ensured with a mass tolerance of less than 1× 10^{-5} error and a false discovery rate of less than 0.01.

Synergistic or antagonistic effects of HE and GA against M^{pro}

The potential drug interaction effects (synergistic, additive, or antagonistic) of HE and GA against SARS-CoV-2 M^{pro} by the combination index (CI), as reported previously. IC_{30}, IC_{50}, and IC_{70} of HE and GA were plotted along the *x* and *y*-axis with the additive lines between them and the combination doses of these compounds marked on the graph area. The synergistic effect of additive lines was shown if the combined dose of each inhibitory concentration was located to the left, and antagonism was demonstrated when it lies to the right, while values near zero demonstrate better synergy [21]. CI was calculated accruing to the classic isobologram Eqn (a) [20, 22].

$$CI = (D)_1/(D_x)_1 + (D)_2/(D_x)_2 \quad \text{(a)}$$

In Eqn (a), D_x and D represent the dose required to achieve 30%, 50%, and 70% inhibition for each drug acting alone and the original dose of the drug in the combination, respectively. CI < 1, CI = 1, and CI > 1 exhibit synergism, additive effect, and antagonism, respectively.

Inactivation kinetic analyses

The inactivation kinetics of HE and GA against SARS-CoV-2 M^{pro} were evaluated using a series of mechanism-based inhibition assays, where varying concentrations of each

inhibitor were incubated for different durations. Initially, a pre-incubation solution containing reaction buffer, various concentrations of inhibitors, and 4 μg·mL^{-1} SARS-CoV-2 M^{pro} was incubated at 37 °C for different pre-incubation times (10, 20, 30, 40, 50, and 60 min). The enzyme reaction was initiated by adding the fluorescent substrate (20 μmol·L^{-1} final concentration), and the resulting fluorescence intensity was measured using a multifunctional microplate reader. The inactivation kinetics data were analyzed using the following Eqn (b) [16, 23, 24].

$$k_{obs} = (k_{inact} * [I])/(K_I + [I]) \quad \text{(b)}$$

In Eqn (b), $[I]$ is initial inactivator concentration, k_{obs} is the observed rate constant of enzyme inactivation, k_{inact} is the maximum potential rate of inactivation, and K_I is the inactivator concentration at half-maximal inactivation rate constant.

Covalent docking simulations

The molecular covalent docking of HE and GA on SARS-CoV-2 M^{pro} was conducted using the covalent docking tools in the Molecular Operating Environment (MOE) 2019.01 [25]. The crystallographic structure of SARS-CoV-2 M^{pro}, available from the Protein Data Bank (PDB Code: 7NBY), was used for molecular docking, and the structure was prepared using the QuickPrep module [15]. HE and GA were constructed in their orthoquinone forms, and their energy was minimized. MarvinSketch was then used to generate covalent reaction formulas for HE/GA and cysteine residues, which were imported into MOE for covalent docking simulations. The docking poses of these generated rigid receptors were refined using the GBVI/WSA dG scoring function to estimate their binding affinity [26]. The initial conformations of the HE-SARS-CoV-2 M^{pro} and GA-SARS-CoV-2 M^{pro} complexes, corresponding to the lowest S-score, were selected for further analysis.

Ensemble docking simulations

Ensemble docking simulations were conducted using AutoDock Vina 1.2.3 [27]. The apo and single-bound structures of SARS-CoV-2 M^{pro} were obtained from the crystal protein structure (PDB Code: 6LU7) in the PDB database. Additionally, holo structures were generated through cluster analysis of dynamic trajectories using the GROMOS method [20]. Both enzyme and ligand structures were preprocessed using AutoDockTools 1.5.7, which included adding polar hydrogen atoms and Gasteiger charges. A grid box of 22.5 Å × 22.5 Å × 22.5 Å with 1 Å spacing was defined at the active site and allosteric site of SARS-CoV-2 M^{pro}. All other parameters were set to their default values.

Molecular dynamics (MD) simulations

The starting coordinates for the apo, single-bound, and di-bound SARS-CoV-2 M^{pro} structures were obtained from the crystal protein structure (PDB Code: 6LU7) in the PDB database. Holo structures were generated through cluster analysis of dynamic trajectories using the GROMOS method. Additionally, the starting coordinates for inhibitors were acquired from docking poses with the lowest predicted binding energy. Coordinate files of SARS-CoV-2 M^{pro} and inhibitors were prepared in the CHARMM36-mar2019 force field [28]. The system was solvated in a cubic box with a minimum distance of 10 Å between the box edge and the M^{pro}/M^{pro}-inhibitor complexes. Water molecules were modeled using the TIP3P model, and 0.15 mol·L^{-1} NaCl was added to neutralize the systems. Each system underwent energy minimization using the steepest descent algorithm with a maximum of 50 000 steps, ensuring the maximum force was lower than 10.0 kJ·mol^{-1}. Temperature was adjusted to 310 K in the NVT ensemble for 100-ps equilibration using the V-rescale thermostat. Subsequently, the NPT ensemble at 1 bar was maintained for an additional 100-ps equilibration using the Parrinello-Rahman barostat. During the production phase, temperature and pressure were maintained at 310 K and 1 bar using the V-rescale thermostat and Parrinello-Rahman barostat. Each system underwent 100-ns MD simulations. Following the simulations, GROMACS 2022 was used to conduct cluster analysis, RMSD, and RMSF analyses on the trajectories [29]. Enzyme-inhibitor interactions were analyzed using Discovery Studio Visualizer (San Diego, USA).

Statistical analysis

The IC$_{50}$ and K_I values were determined using GraphPad Prism 7.0 software (GraphPad Software, Inc., La Jolla, USA) and expressed as mean ± SD. Raw NanoLC-MS/MS data were searched against peptide databases using Protein Discovery 2.4 (Thermo Scientific, Waltham, MA) with the Sequest HT algorithm. The data were then converted to mgf format using MSconvert software, and MS^2 spectra were outputted using pLabel v2.4.1 software.

Results

Inhibition of SARS-CoV-2 M^{pro} by ENA

Initially, the preliminary inhibitory effects of 21 herbs in Qingfei Paidu decoction on SARS-CoV-2 M^{pro}-catalyzed DKE enzymatic activity were studied. The results showed that ESE exhibited potent inhibition activity against SARS-CoV-2 M^{pro}, with a calculated IC$_{50}$ value of 86.79 μg·mL^{-1} (Figs. 1A, S2, & S3). To identify strong SARS-CoV-2 M^{pro} inhibitors from Ephedra, we isolated and purified the alkaloid and non-alkaloid fractions of Ephedra, with the detailed extraction process provided in the supporting material. The inhibitory effects of these fractions on SARS-CoV-2 M^{pro} were then assayed. Surprisingly, the residual activity of SARS-CoV-2 M^{pro} was almost completely inhibited in the presence of the ENA at a dose of 100 μg·mL^{-1} (Fig. 1B), while the Ephedra alkaloid fraction had a negligible impact on SARS-CoV-2 M^{pro}. As depicted in Fig. 2, time-dependent inhibition assays revealed that ENA inhibited SARS-CoV-2 M^{pro} enzymatic activity in a dose- and time-dependent manner. Notably, as the pre-incubation time of ENA with SARS-CoV-2 M^{pro} increased, the apparent IC$_{50}$ value dramatically decreased, with an IC$_{50}$ of 4.58 μg·mL^{-1} following a 60-minute pre-incubation. This shift implies that some constituents in ENA might act as covalent binders of SARS-

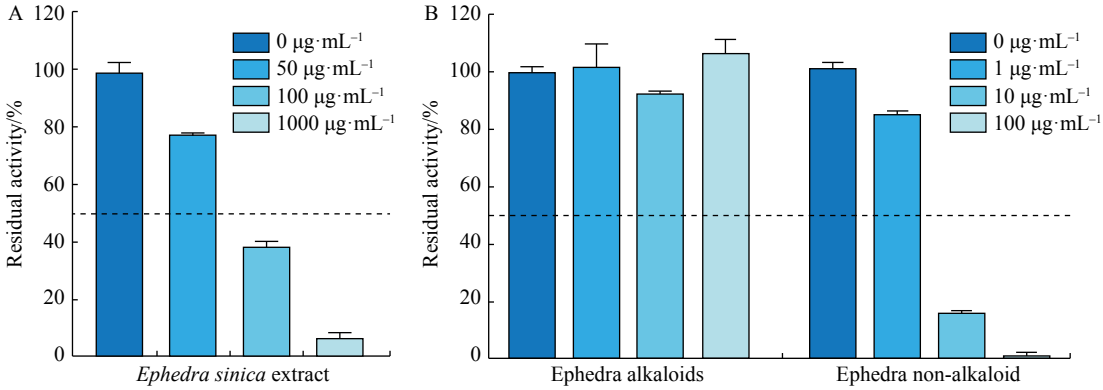

Fig. 1 (A) The anti-SARS-CoV-2 M^{pro} effects of *Ephedra sinica* extract. (B) The anti-SARS-CoV-2 M^{pro} effects of two fractions isolated from *Ephedra sinica* extract including total alkaloids and non-alkaloid fraction. Data are expressed as mean ± SD (n = 3).

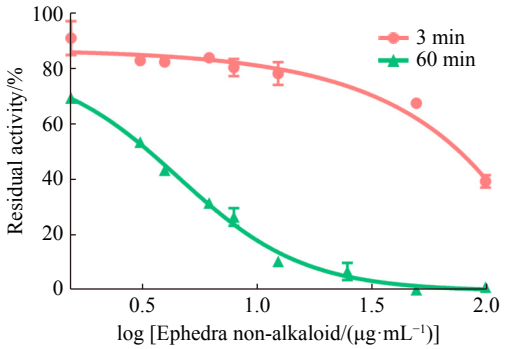

Fig. 2 Dose- and time-dependent inhibition curves of Ephedra non-alkaloid fraction against SARS-CoV-2 M^{pro} with different pre-incubation times (3 min and 60 min). Data are expressed as mean ± SD (n = 3).

CoV-2 M^{pro} [16, 17].

Inhibition of SARS-CoV-2 M^{pro} by the constituents in ENA

To characterize the key constituents in the ENA, UHPLC-Q-Exactive Orbitrap HRMS was employed. As shown in Table S2 and Fig. S4, the constituents were identified using standards by comparing their retention times (t_R), UV spectra, and MS_2 spectra. Sixteen commercially available constituents in ENA were collected (Fig. S5), including ferulic acid, GA, tricin, isovitexin, vitexin, rutin, quercitrin, isoquercitrin, kaempferol, apigenin, quercetin, HE, catechin, epicatechin, naringenin, and taxifolin. The inhibition effects of these monomeric compounds from the non-alkaloidal fraction of Ephedra on SARS-CoV-2 M^{pro}'s hydrolytic activity were investigated. Initial screening experiments were conducted to determine the inhibition potentials of these constituents on SARS-CoV-2 M^{pro}. As shown in Fig. 3, HE and GA displayed significant effectiveness against SARS-CoV-2 M^{pro}, with IC_{50} values ranging from 0 to 10 μmol·L^{-1}. Quercetin, tricin, and apigenin exhibited moderate inhibition, with IC_{50} values between 10 and 100 μmol·L^{-1}. The dose- and time-dependent inhibition curves for these constituents, as well as for the positive inhibitors dihydromyricetin and ebselen against SARS-CoV-2 M^{pro} are listed in Table 1 and Fig. 4. Among all tested compounds, HE, GA, quercetin, tricin, and apigenin significantly inhibited SARS-CoV-2 M^{pro} after 60 min pre-incubation, with the IC_{50} values of 3.33, 5.98, 19.73, 17.48, 56.94 μmol·L^{-1}, respectively. Furthermore, an isobologram approach and CI values were employed to assess the synergistic or antagonistic effects of HE and GA on SARS-CoV-2 M^{pro} [30]. As shown in Fig. 5, Table S3, and Table S4, the results demonstrated that the combination of HE and GA exhibited more potent anti-SARS-CoV-2 M^{pro} effects, indicating that these two bioactive constituents showed synergistic effects (rather than additive or antagonistic effects) against SARS-CoV-2 M^{pro}.

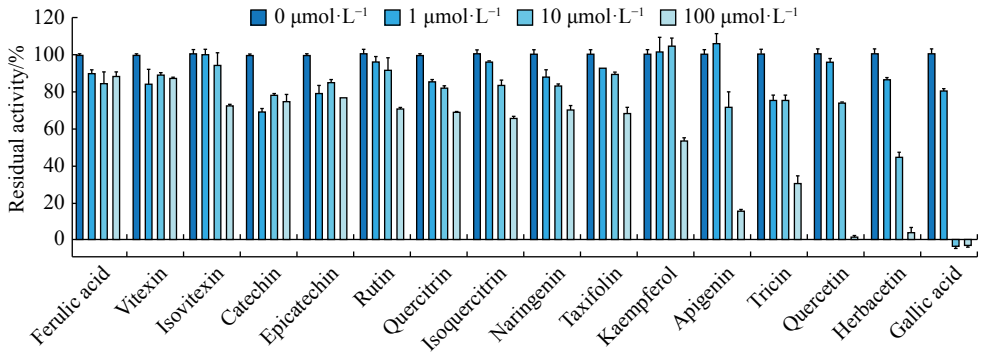

Fig. 3 The anti-SARS-CoV-2 M^{pro} effects of the major constituents (0, 1, 10, 100 μmol·L^{-1}) isolated from non-alkaloid fraction of Ephedra. Data are expressed as mean ± SD (n = 3).

Table 1 IC_{50} values of Ephedra non-alkaloid and its five active constituents against SARS-CoV-2 M^{pro}

No.	Compound	M_r	Structure	IC_{50} (μmol·L^{-1})		Ratio	K_I (μmol·L^{-1})	K_{inact} (min^{-1})
				3 min	60 min			
1	Herbacetin	302.24	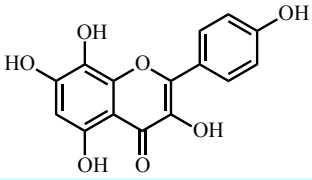	57.75	3.33	17.34	18.87	0.01
2	Gallic acid	170.12	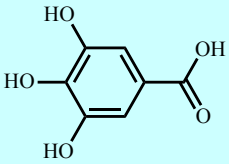	> 100	5.98	> 16.72	35.38	0.15
3	Quercetin	302.24	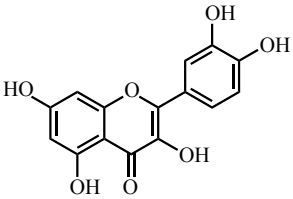	63.48	19.73	3.22	–	–
4	Tricin	330.3	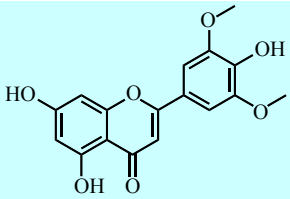	66.04	17.48	3.78	–	–
5	Apigenin	270.24	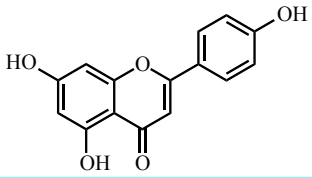	> 100	56.94	> 1.76	–	–
6	Dihydromyricetin[a]	318.24	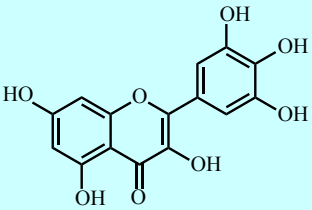	10.55	3.33	3.17	–	–
7	Ebselen[a]	274.18	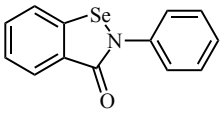	1.33	1.03	1.29	–	–

* Dihydromyricetin and Ebselen were used as positive inhibitors of SARS-CoV-2 M^{pro}.

Inactivation kinetics of HE and GA on SARS-CoV-2 M^{pro}

Given the effective inhibitory potential of HE and GA against SARS-CoV-2 M^{pro}, as well as their significant synergistic effects when combined, we further investigated their inactivation kinetics to assess their inactivation potency. Previously, time-dependent inhibition assays were conducted to explore the inhibition mechanism of these compounds by comparing the IC_{50} values at different incubation times (with a fold change > 16.7). In this study, various concentrations of the inhibitors were used with varying incubation times to plot the inactivation kinetic curves. As shown in Fig. 6, HE and GA both inactivated the activity of SARS-CoV-2 M^{pro} in a dose- and time-dependent manner. The K_I values were determined to be 18.87 μmol·L^{-1} for HE and 35.38 μmol·L^{-1} for GA. In conclusion, HE and GA were identified as natural time-dependent inhibitors of SARS-CoV-2 M^{pro}, with HE demonstrating the strongest inactivation potency. HE was found to covalently bind to M^{pro}, acting as an irreversible in-

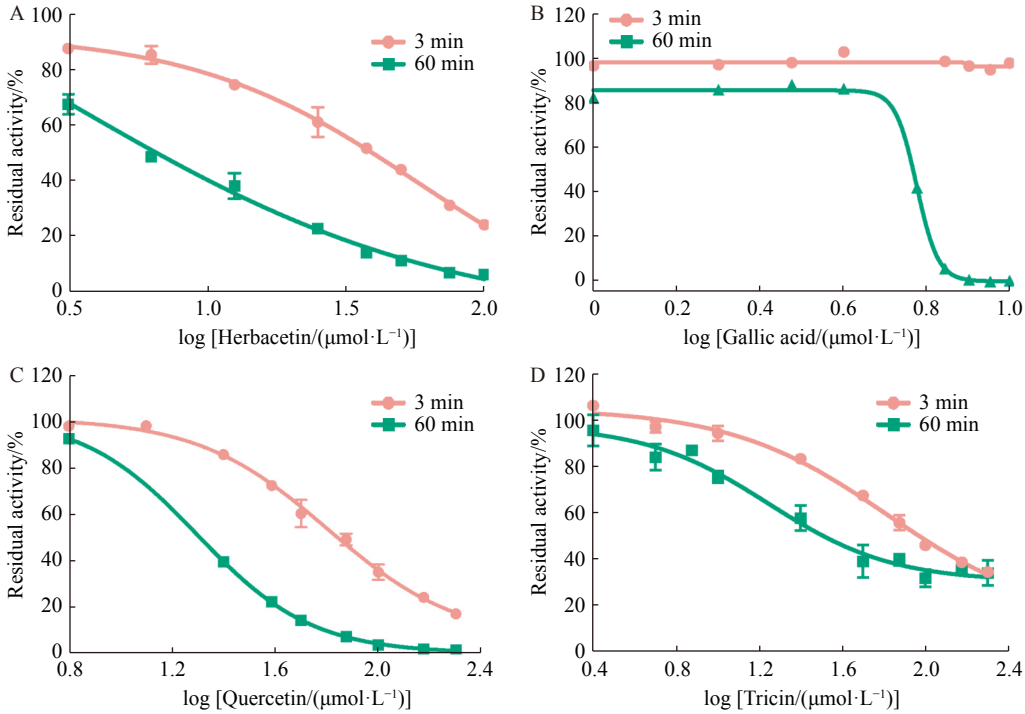

Fig. 4 Dose- and time-dependent inhibition curves of HE (A), GA (B), quercetin (C), and tricin (D) against SARS-CoV-2 M^{pro}. Data are expressed as mean ± SD (n = 3).

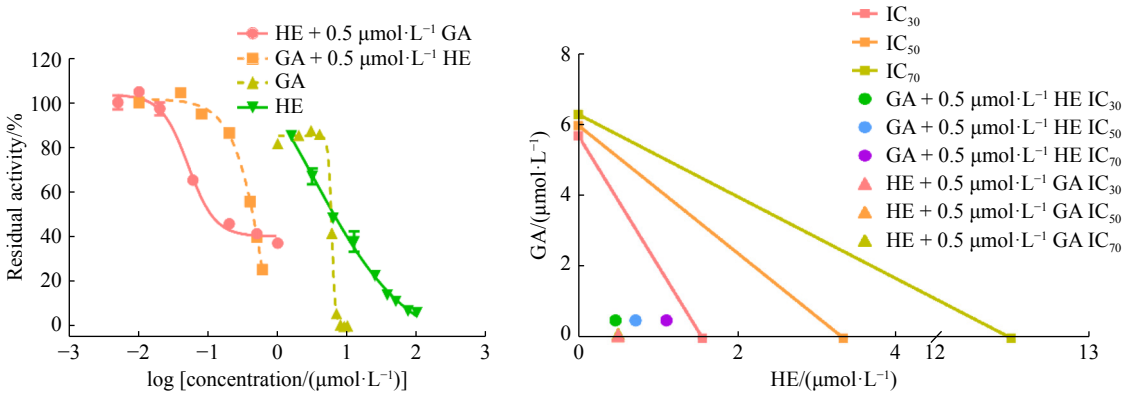

Fig. 5 (A-B) Antagonism and synergism graph of HE and GA against SARS-CoV-2 M^{pro}. Data are expressed as mean ± SD (n = 3).

hibitor. These findings prompted further investigation into the interaction patterns between these agents and SARS-CoV-2 M^{pro}, enhancing our understanding of their potential therapeutic applications.

Identification of the modified sites of HE and GA on SARS-CoV-2 M^{pro}

Next, we identified the covalent binding sites of HE and GA on SARS-CoV-2 M^{pro} using mass spectrometry. Structurally, these compounds contain one or more catechol moieties that can be readily oxidized to form *o*-quinones *via* a two-electron transfer process. These *o*-quinones are capable of covalently binding to essential cysteines of SARS-CoV-2 M^{pro} [15]. By systematically searching for the characteristic fragments of labeled peptides on cysteines of M^{pro}, the MS^2 spectra of HE (+302.042 65 Da) and GA (+168.005 87 Da) were generated. The predicted b- and y-type ions were listed above and below the peptide sequence. As shown in Table 2 & Figs. S6–S8, both HE and GA could covalently modify the peptide HVICTSEDMLNPNYEDLLIR at Cys44 *via* their orthoquinone forms. Additionally, HE could also covalently modify the peptide VIGHSMQNCVLK at Cys85. Notably, previous investigations have indicated that both Cys85 and Cys44 are crucial functional cysteines of SARS-CoV-2 M^{pro}, which are tightly associated with the enzymatic activity of this key enzyme [31-33]. These findings suggest that HE and GA could inactivate SARS-CoV-2 M^{pro} by covalently modifying these functional cysteines, thus impairing the enzymatic activity of this critical viral protease.

Covalent docking simulations

To further elucidate the potential ligand binding sites and

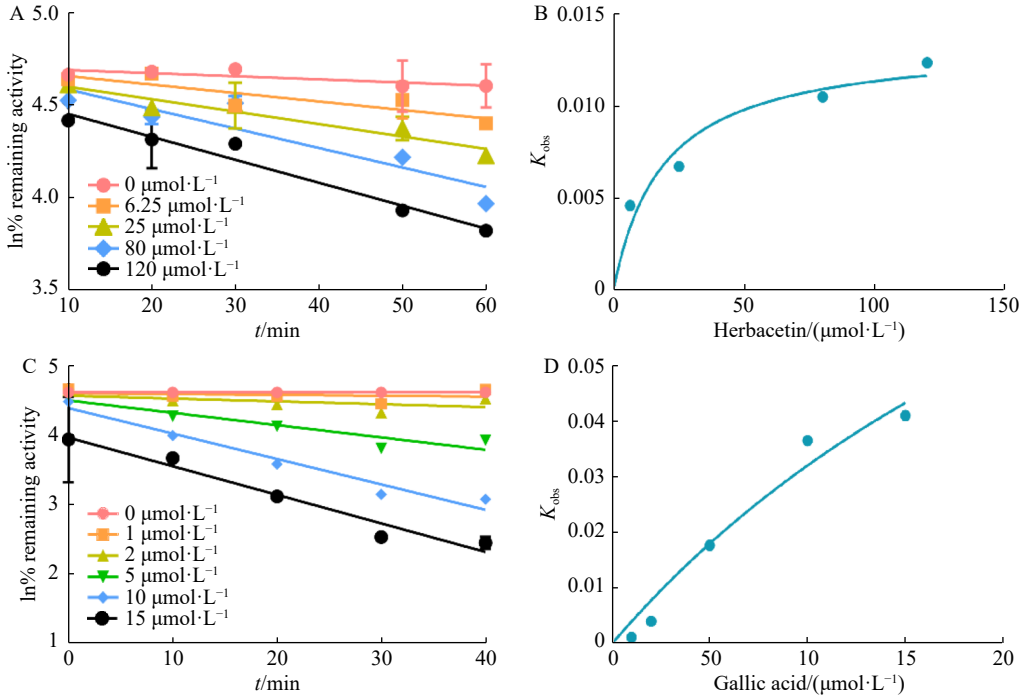

Fig. 6 (A) Inactivation kinetics of SARS-CoV-2 M^{pro} by HE. (B) The hyperbolic plot of k_{obs} of SARS-CoV-2 M^{pro} *vs* HE concentrations. (C) Inactivation kinetics of SARS-CoV-2 M^{pro} by GA. (D) The hyperbolic plot of k_{obs} of SARS-CoV-2 M^{pro} *vs* GA concentrations. Data are expressed as mean ± SD (n = 3).

interaction patterns of HE and GA with SARS-CoV-2 M^{pro}, these inhibitors were covalently docked into the three-dimensional structure of M^{pro} (PDB: 7NBY) using MOE's covalent docking module. HE was found to covalently bind to both Cys44 and Cys85, while GA covalently modified Cys44 of M^{pro}. As depicted in Figs. S9 and S11, HE forms covalent adducts with Cys44 and Cys85. The covalent modification of Cys44 by HE allows the formation of hydrogen bonds with key residues Met49 and Met165, which surround the catalytic site, thus showing outstanding binding affinity. Following the covalent modification of Cys85, HE can interact with Asp187, Asn53, and Glu55 *via* hydrogen bonding. Similarly, GA forms hydrogen bonds with Cys44 and Met49 after covalently modifying Cys44. Additionally, GA forms carbon-hydrogen bonds with Met49 and Asp188. Consequently, both HE and GA interact with several key residues in the catalytic region of M^{pro}. HE, in particular, stably binds at multiple sites to the sulfhydryl groups of cysteine, acting as a powerful irreversible inhibitor. These findings suggest that HE and GA inhibit SARS-CoV-2 M^{pro} through covalent modifications, which enable strong interactions with the enzyme's catalytic residues, thereby impairing its enzymatic activity and offering potential therapeutic applications.

MD simulations

To further explore the inactivation mechanism of HE, MD simulations were conducted. We simulated both one-to-one (HE-M^{pro}) and two-to-one (2 HE-M^{pro}) binding modes at the Cys44 site (located at the active site) and the Cys85 site (defined as the allosteric site) in a water solvent containing 0.15 mol·L^{-1} NaCl [33]. As shown in Fig. 7A, RMSD analysis for ligand molecules in different binding modes indicated that HE could bind stably to the active site in both one-to-one and two-to-one binding modes during molecular dynamics simulations, with flattened RMSD fluctuations from 40 to 100 ns. However, HE exhibited volatile RMSD distribution when interacting solely with the allosteric site of SARS-CoV-2 M^{pro}. This suggests that HE binding at the active site induces the formation of an additional HE-binding pocket at Cys85. Cluster analysis of di-bound M^{pro} was conducted using the GROMOS method, and the enzyme-inhibitor interactions of the largest middle structure were further analyzed. As shown in Figs. 7B & S12, HE was immobilized at the active site primarily through hydrogen bonds with Thr45, Gly143, Ser144, Cys145, Glu166, and Gln189. Since Cys145 is a crucial catalytic residue and Gly143-Cys145 constitutes the oxyanion hole essential for substrate recognition, the binding of HE to the active site would hinder the enzymatic activity of SARS-CoV-2 M^{pro} [17]. At the allosteric site, HE was well accommodated through electrostatic and hydrophobic interactions, including π-cation, π-anion, π-σ, π-π stacked, and π-alkyl interactions (Fig. 7C). RMSF distribution analysis of apo, single-bound, and di-bound SARS-CoV-2 M^{pro} was performed to search for structural transformations induced by HE binding. As shown in Fig. 7D, two regions with relatively high flexibility—the P5 loop (residues 180–200) and the C-terminal of SARS-CoV-2 M^{pro}—were stabilized when HE bound to the active site. However, additional binding at the allosteric site decreased the structural stability of the P2

Table 2 Identification of the covalent binding sites for HE and GA on SARS-CoV-2 M^{pro} by nanoLC-MS/MS

Inhibitor	Peptide	Modification	Charge	(*m/z*)/Da	MH^+/Da	Theo. MH^+/Da	Error	t_R/min
Herbacetin	CPRHVICTSEDMLNPNYEDLLIR	Cys44	4	826.609 01	3 303.414 21	3 303.395 53	5.65	55.332
	VIGHSMQNCVLK	Cys85	2	815.868 84	1 630.730 39	1 630.723 99	3.93	47.152
Gallic acid	HVICTSEDMLNPNYEDLLIR	Cys44	3	853.722 35	2 559.152 50	2 559.137 78	5.75	58.648

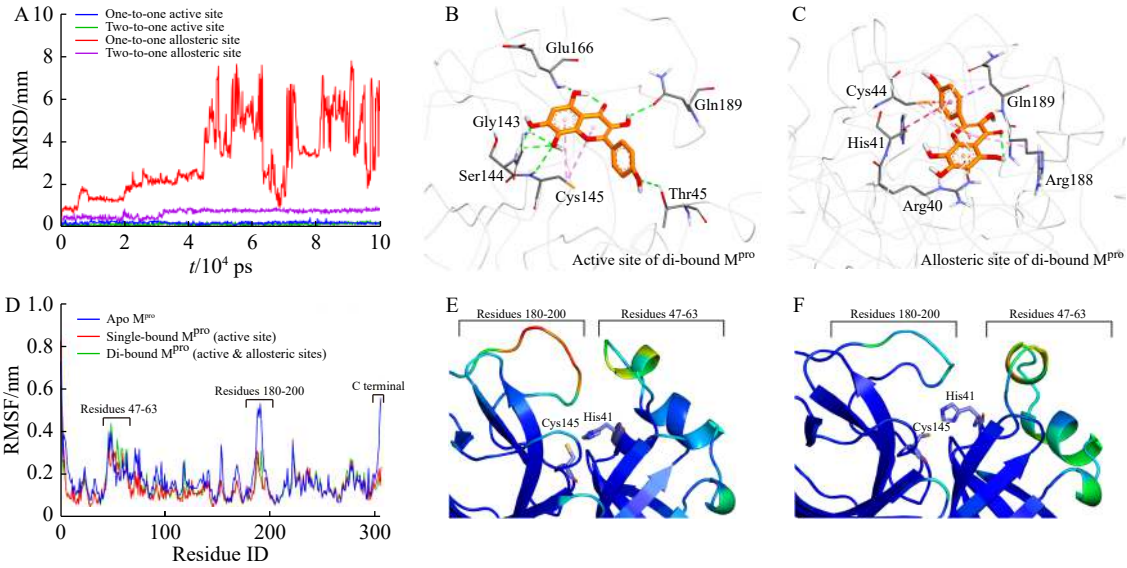

Fig. 7 (A) RMSD analysis of HE binding to the active and allosteric sites on M^{pro} *via* one-to-one mode (HE-M^{pro}) and two-to-one mode (2 HE-M^{pro}). (B and C) 3D enzyme-inhibitor analysis of the largest middle structure of di-bound M^{pro}-HE (2 HE-M^{pro}) at the active site and allosteric site. (D) RMSF analysis of protein structure of apo, single-bound, and di-bound M^{pro}. (E and F) Active pockets of apo and di-bound M^{pro} were colored according to the B factor values. Red→Blue should be matched to unstable→stable structural region. Catalytic dyad $Cys145^-$-$His41^+$ was labeled.

helix, consisting of residues 47-63 (Figs. 7E and 7F) [34]. The P2 helix and P5 loop are among the most dynamic regions in M^{pro}, and the conserved Asp187 on the P5 loop plays a significant role in maintaining the positive charge of catalytic His41 [34]. Thus, disturbing the plasticity of the P2 helix and P5 loop could reduce SARS-CoV-2 M^{pro}'s ability to accommodate various ligands and hydrolyze substrates.

Discussion

A devastating epidemic, COVID-19, is caused by the highly transmissible SARS-CoV-2, necessitating more effective therapeutic strategies [35, 36]. Among all validated anti-CoVs targets, M^{pro}, a class of highly conserved cysteine hydrolases, is widely recognized as a key target for preventing and treating CoVs-related diseases [37, 38]. In recent years, CMs have become routine treatments for pandemic and endemic diseases, including COVID-19. Despite the existence of several marketed CMs, such as Qingfei Paidu decoction and Lianhua Qingwen capsule, which play a crucial role in treating COVID-19 [39, 40], identifying the major phytochemicals responsible for their antiviral activity remains a significant challenge.

Ephedra plays a crucial role in the formulation of renowned CMs used to treat respiratory ailments like colds, coughs, and asthma [41-43]. Notably, the alkaloid fraction of Ephedra has undergone extensive investigation due to its effectiveness in treating asthma and its anti-influenza properties [44]. However, the non-alkaloid fractions of Ephedra, which have shown anti-asthmatic, anti-influenza, hypoglycemic, hypolipidemic, and antioxidant effects without causing adverse reactions such as arrhythmia or insomnia associated with ephedra alkaloids, have garnered less attention [45]. To summarize, Ephedra demonstrates anti-COVID-19 effects as an antipyretic, analgesic, cathartic, and asthma treatment [41]. Additionally, it has been reported that Ephedra, along with its alkaloid components —ephedrine, pseudoephedrine, and methylephedrine—binds with ACE2 in a specific manner to some amino acid residues, reducing the entrance ratio of pseudovirus in a pseudovirus model, thus exhibiting anti-CoV effects [10]. However, the anti-SARS-CoV-2 M^{pro} substances within Ephedra and their action mechanisms have not been fully revealed.

To identify potent SARS-CoV-2 M^{pro} covalent inhibitors, a high-throughput screening assay was conducted. The ESE was found to significantly inhibit the hydrolytic activity of SARS-CoV-2 M^{pro}. Given that the primary pharmacodynamic constituents of Ephedra include both alkaloids and non-alkaloids, the subsequent isolation of non-alkaloid fractions

from Ephedra revealed a substantial anti-M^{pro} effect in a time- and dose-dependent manner. In contrast, the Ephedra alkaloid fractions exhibited weak inhibitory effects on SARS-CoV-2 M^{pro}. Consequently, further investigations focused on the non-alkaloid fractions of Ephedra. Notably, while Ephedra alkaloids have anti-inflammatory and antipyretic properties that may alleviate symptoms associated with emerging viral infections, this study highlighted the significant inhibitory effects of the ENA on SARS-CoV-2 M^{pro}. This provides strong evidence supporting the anti-CoV effects of the antiviral herb Ephedra in combating COVID-19. Future research could explore the synergistic effects of multi-constituents and multi-targets within both fractions.

Among all tested constituents, HE and GA in ENA demonstrated time- and dose-dependent inhibition of SARS-CoV-2 M^{pro}. Notably, their combination exhibited a significant synergistic effect on this key enzyme. GA intensified the effects of HE, remarkably reducing the IC_{50} from approximately 3.33 μmol·L^{-1} to 60.0 nmol·L^{-1}, representing more than a 55-fold change. Similarly, the IC_{50} of GA decreased by over 8-fold in synergy with HE. These findings provide valuable insights into the heightened synergy of active constituents in Ephedra, offering strong evidence for its anti-coronavirus effects. Currently, various inhibitors targeting SARS-CoV-2 M^{pro} have been identified [17, 46]. These inhibitors can be categorized into covalent and non-covalent inhibitors based on their mechanisms of inhibition [47]. Theoretically, combining two covalent inhibitors could provide more effective M^{pro} blockade by targeting different ligand-binding sites. Additionally, combining covalent and non-covalent inhibitors could induce conformational changes in the non-covalent inhibitors upon binding to SARS-CoV-2 M^{pro}, potentially exposing internal cysteines. Such combinations could offer synergistic or additive effects during COVID-19 treatments.

Conclusion

This study revealed that the antiviral herb ESE and its ENA strongly inhibited SARS-CoV-2 M^{pro} in time- and dose-dependent manners. The chemical constituents in the non-alkaloid fraction of ESE were comprehensively analyzed, and the anti-SARS-CoV-2 M^{pro} effects of the major constituents in ENA were evaluated. Among the 16 phytochemicals isolated from ENA, HE and GA exhibited strong inhibitory effects on M^{pro}, with IC_{50} values of 3.33 and 5.98 μmol·L^{-1}, respectively, after a 60-minute pre-incubation. Interestingly, the combination of HE and GA showed significant synergistic anti-M^{pro} effects. Inhibition kinetic assays demonstrated that HE and GA efficiently inactivated M^{pro}. Mass spectrometry-based peptide profiling revealed that HE covalently modified two crucial cysteines (Cys44 and Cys85) of M^{pro}, while GA covalently modified SARS-CoV-2 M^{pro} at Cys44. Molecular dynamics simulations were conducted to explore the inhibitory mechanisms of HE binding covalently to Cys44 and Cys85 of SARS-CoV-2 M^{pro}. Collectively, these findings elucidate the active anti-SARS-CoV-2 M^{pro} constituents from Ephedra and their inhibitory mechanisms. This provides significant evidence to support the anti-CoV effects of the antiviral herb Ephedra and offers new insights into the design and development of novel therapeutic strategies for treating CoV-related epidemics, including COVID-19.

Supporting Information

supporting data can be requested by sending E-mail to the corresponding authors.

References

[1] Xie X, Hu L, Xue H, *et al*. Prognosis and treatment of complications associated with COVID-19: a systematic review and meta-analysis [J]. *Acta Mat Med*, 2022, **1**(1): 124-137.

[2] Zhang L, Lin D, Sun X, *et al*. Crystal structure of SARS-CoV-2 main protease provides a basis for design of improved alpha-ketoamide inhibitors [J]. *Science*, 2020, **368**(6489): 409-412.

[3] Wang X, Ma S, Zhao B, *et al*. Correlations between the viral loads and symptoms in the SARS-CoV-2-infected patients [J]. *MedComm (2020)*, 2023, **4**(4): e324.

[4] Manjunath SH, Thimmulappa RK. Antiviral, immunomodulatory, and anticoagulant effects of quercetin and its derivatives: potential role in prevention and management of COVID-19 [J]. *J Pharm Anal*, 2022, **12**(1): 29-34.

[5] Ni L, Chen L, Huang X, *et al*. Combating COVID-19 with integrated traditional Chinese and Western medicine in China [J]. *Acta Pharm Sin B*, 2020, **10**(7): 1149-1162.

[6] Ji X, Meng X, Zhu X, *et al*. Research and development of Chinese anti-COVID-19 drugs [J]. *Acta Pharm Sin B*, 2022, **12**(12): 4271-4286.

[7] Chen J, Wang YK, Gao Y, *et al*. Protection against COVID-19 injury by qingfei paidu decoction *via* anti-viral, anti-inflammatory activity and metabolic programming [J]. *Biomed Pharmacother*, 2020, **129**: 110281.

[8] Lee DYW, Li QY, Liu J, *et al*. Traditional Chinese herbal medicine at the forefront battle against COVID-19: clinical experience and scientific basis [J]. *Phytomedicine*, 2021, **80**: 153337.

[9] Yang Y, Islam MS, Wang J, *et al*. Traditional Chinese medicine in the treatment of patients infected with 2019-New Coronavirus (SARS-CoV-2): a review and perspective [J]. *Int J Biol Sci*, 2020, **16**(10): 1708-1717.

[10] Lv Y, Wang S, Liang P, *et al*. Screening and evaluation of anti-SARS-CoV-2 components from *Ephedra sinica* by ACE2/CMC-HPLC-IT-TOF-MS approach [J]. *Anal Bioanal Chem*, 2021, **413**(11): 2995-3004.

[11] Zhong LLD, Lam WC, Yang W, *et al*. Potential targets for treatment of Coronavirus Disease 2019 (COVID-19): a review of Qing-Fei-Pai-Du-Tang and its major herbs [J]. *Am J Chin Med*, 2020, **48**(5): 1051-1071.

[12] Qiao J, Li YS, Zeng R, *et al*. SARS-CoV-2 M^{pro} inhibitors with antiviral activity in a transgenic mouse model [J]. *Science*, 2021, **371**(6536): 1374-1378.

[13] Zhou Z, Zhu Y, Chu M. Role of COVID-19 vaccines in SARS-CoV-2 variants [J]. *Front Immunol*, 2022, **13**: 898192.

[14] Shrestha LB, Foster C, Rawlinson W, *et al*. Evolution of the SARS-CoV-2 omicron variants BA. 1 to BA. 5: implications for immune escape and transmission [J]. *Rev Med Virol*, 2022, **32**(5): e2381.

[15] Cao Y, Jian F, Wang J, *et al*. Imprinted SARS-CoV-2 humoral immunity induces convergent Omicron RBD evolution [J]. *Nature*, 2023, **614**(7948): 521-529.

[16] Xiong Y, Zhu GH, Zhang YN, *et al*. Flavonoids in *Ampelopsis*

grossedentata as covalent inhibitors of SARS-CoV-2 3CL^{pro}: inhibition potentials, covalent binding sites and inhibitory mechanisms [J]. *Int J Biol Macromol*, 2021, **187**: 976-987.

[17] Hu Q, Xiong Y, Zhu GH, *et al*. The SARS-CoV-2 main protease (M^{pro}): structure, function, and emerging therapies for COVID-19 [J]. *MedComm (2020)*, 2022, **3**(3): e151.

[18] Zhang YN, Zhu GH, Liu W, *et al*. Discovery and characterization of the covalent SARS-CoV-2 3CL^{pro} inhibitors from *Ginkgo biloba* extract *via* integrating chemoproteomic and biochemical approaches [J]. *Phytomedicine*, 2023, **114**: 154796.

[19] Sutanto F, Konstantinidou M, Dömling A. Covalent inhibitors: a rational approach to drug discovery [J]. *RSC Med Chem*, 2020, **11**(8): 876-884.

[20] Jin Z, Du X, Xu Y, *et al*. Structure of M^{pro} from SARS-CoV-2 and discovery of its inhibitors [J]. *Nature*, 2020, **582**(7811): 289-293.

[21] Sadeghi S, Valadkhani Z, Tafreshi AS, *et al*. A study of synergy of combination of eosin B with chloroquine, artemisinin, and sulphadoxine-pyrimethamine on *Plasmodium falciparum in vitro* and *Plasmodium berghei in vivo* [J]. *J Trop Med*, 2020, **2020**: 3013701.

[22] Son HU, Yoon EK, Yoo CY, *et al*. Effects of synergistic inhibition on *α*-glucosidase by phytoalexins in soybeans [J]. *Biomolecules*, 2019, **9**(12): 828.

[23] Polasek TM, Elliot DJ, Somogyi AA, *et al*. An evaluation of potential mechanism-based inactivation of human drug metabolizing cytochromes P450 by monoamine oxidase inhibitors, including isoniazid [J]. *Br J Clin Pharmacol*, 2006, **61**(5): 570-584.

[24] Zhang F, Liu W, Huang J, *et al*. Inhibition of drug-metabolizing enzymes by Jingyin granules: implications of herb–drug interactions in antiviral therapy [J]. *Acta Pharmacol Sin*, 2021, **43**(4): 1072-1081.

[25] Paul AS, Islam R, Parves MR, *et al*. Cysteine focused covalent inhibitors against the main protease of SARS-CoV-2 [J]. *J Biomol Struct Dyn*, 2022, **40**(4): 1639-1658.

[26] Labute P. The generalized Born/volume integral implicit solvent model: estimation of the free energy of hydration using London dispersion instead of atomic surface area [J]. *J Comput Chem*, 2008, **29**(10): 1693-1698.

[27] Eberhardt J, Santos-Martins D, Tillack AF, *et al*. AutoDock Vina 1.2.0: new docking methods, expanded force field, and python bindings [J]. *J Chem Inf Model*, 2021, **61**(8): 3891-3898.

[28] Huang J, Rauscher S, Nawrocki G, *et al*. CHARMM36m: an improved force field for folded and intrinsically disordered proteins [J]. *Nat Methods*, 2016, **14**(1): 71-73.

[29] Van Der Spoel D, Lindahl E, Hess B, *et al*. GROMACS: fast, flexible, and free [J]. *J Comput Chem*, 2005, **26**(16): 1701-1718.

[30] Huang RY, Pei L, Liu Q, *et al*. Isobologram analysis: a comprehensive review of methodology and current research [J]. *Front Pharmacol*, 2019, **10**: 1222.

[31] Verma N, Henderson JA, Shen J. Proton-coupled conformational activation of SARS coronavirus main proteases and opportunity for designing small-molecule broad-spectrum targeted covalent inhibitors [J]. *J Am Chem Soc*, 2020, **142**(52): 21883-21890.

[32] Du L, Xie Y, Zheng K, *et al*. Oxidative stress transforms 3CL^{pro} into an insoluble and more active form to promote SARS-CoV-2 replication [J]. *Redox Biol*, 2021, **48**: 102199.

[33] Ravanfar R, Sheng Y, Shahgholi M, *et al*. Surface cysteines could protect the SARS-CoV-2 main protease from oxidative damage [J]. *J Inorg Biochem*, 2022, **234**: 111886.

[34] Kneller DW, Phillips G, O'Neill HM, *et al*. Room-temperature X-ray crystallography reveals the oxidation and reactivity of cysteine residues in SARS-CoV-2 3CL M^{pro}: insights into enzyme mechanism and drug design [J]. *IUCrJ*, 2020, **7**(6): 1028-1035.

[35] Puhach O, Meyer B, Eckerle I. SARS-CoV-2 viral load and shedding kinetics [J]. *Nat Rev Microbiol*, 2023, **21**(3): 147-161.

[36] Li J, Lai S, Gao GF, *et al*. The emergence, genomic diversity and global spread of SARS-CoV-2 [J]. *Nature*, 2021, **600**(7889): 408-418.

[37] Avila-Galvez MA, Rafael-Pita C, Fernandez N, *et al*. Targeting proteases involved in the viral replication of SARS-CoV-2 by sesquiterpene lactones from chicory (*Cichorium intybus* L.) [J]. *Food Funct*, 2022, **13**(17): 8977-8988.

[38] Hameedi MA, Prates ET, Garvin MR, *et al*. Structural and functional characterization of NEMO cleavage by SARS-CoV-2 3CLpro [J]. *BioRxiv*, 2021, **13**(1): 5285.

[39] Li Y, Chu F, Li P, *et al*. Potential effect of Maxing Shigan decoction against coronavirus disease 2019 (COVID-19) revealed by network pharmacology and experimental verification [J]. *J Ethnopharmacol*, 2021, **271**: 113854.

[40] Zheng Y, Shi C, Han Y, *et al*. Efficacy and safety of a Chinese herbal formula Maxing Ganshi Decoction in children with community-acquired pneumonia: a randomized, double-blind, placebo-controlled, multicenter trial [J]. *Front Pharmacol*, 2022, **13**: 948831.

[41] Mei J, Zhou Y, Yang X, *et al*. Active components in *Ephedra sinica* Stapf disrupt the interaction between ACE2 and SARS-CoV-2 RBD: potent COVID-19 therapeutic agents [J]. *J Ethnopharmacol*, 2021, **278**: 114303.

[42] Zheng Q, Mu X, Pan S, *et al*. Ephedrae herba: a comprehensive review of its traditional uses, phytochemistry, pharmacology, and toxicology [J]. *J Ethnopharmacol*, 2023, **307**: 116153.

[43] Zhang BM, Wang ZB, Xin P, *et al*. Phytochemistry and pharmacology of genus *Ephedra* [J]. *Chin J Nat Med*, 2018, **16**(11): 811-828.

[44] Tang S, Ren J, Kong L, *et al*. Ephedrae herba: a review of its phytochemistry, pharmacology, clinical application, and alkaloid toxicity [J]. *Molecules*, 2023, **28**(2): 663.

[45] Hyuga S, Hyuga M, Oshima N, *et al*. Ephedrine alkaloids-free Ephedra Herb extract: a safer alternative to ephedra with comparable analgesic, anticancer, and anti-influenza activities [J]. *J Nat Med*, 2016, **70**(3): 571-583.

[46] Mody V, Ho J, Wills S, *et al*. Identification of 3-chymotrypsin like protease (3CLPro) inhibitors as potential anti-SARS-CoV-2 agents [J]. *Commun Biol*, 2021, **4**(1): 93.

[47] Feng T, Zhang M, Xu Q, *et al*. Exploration of molecular targets and mechanisms of Chinese medicinal formula Acacia Catechu -Scutellariae Radix in the treatment of COVID-19 by a systems pharmacology strategy [J]. *Phytother Res*, 2022, **36**(11): 4210-4229.

Cite this article as: HU Qing, ZHANG Yiwen, CHEN Pengcheng, *et al*. Discovery and characterization of naturally occurring covalent inhibitors of SARS-CoV-2 M^{pro} from the antiviral herb Ephedra [J]. *Chin J Nat Med*, 2024, **22**(9): 797-807.